Thermooxidative decomposition of oil shales

Tiit Kaljuvee · Merli Keelmann · Andres Trikkel ·
Rein Kuusik

Abstract The thermooxidative decomposition of four oil shale samples from Estonia, Jordan, Israel and Morocco and one sample of Estonian oil shale derivative, semicoke, was studied with the aim to determine the characteristics of the process and the differences of it related to the origin of oil shale. The experiments with a Setaram Setsys 1750 thermoanalyzer coupled to a Nicolet 380 FTIR Spectrometer were carried out under non-isothermal conditions up to 1000 °C at the heating rates of 1, 2, 5, 10 and 20 °C min^{-1} in an oxidizing atmosphere. A model-free kinetic analysis approach based on the differential isoconversional method of Friedman was used to calculate the kinetic parameters. The results of TG–DTA–FTIR analyses and the variation of activation energy E along the reaction progress α indicated the complex character of thermooxidative decomposition of oil shale and semicoke, being at that the most complicated for Estonian and Jordanian oil shale characterized by higher content of organic matter as compared to the other samples studied.

Keywords Kinetics · Oil shale · Semicoke · TG–DTA–FTIR · Thermooxidative decomposition

Introduction

Oil shales (OS) are fine-grade sedimentary rocks containing relatively large amounts of combustible organic matter (kerogen) in mineral matrix. The amount and composition of organic matter as well as the composition of mineral part of it influence the quality of oil shale and determine possibilities of its utilization as a raw material for chemical and/or power industry. The potential resources of OS in the world are enormous, 10–12 trillion tons, and the biggest of them are concentrated in USA, Russian Federation, Congo, Brazil, China, etc. Active exploitation of OS takes place in Estonia (for electricity generation and for shale oil production), Brazil (shale oil), China (shale oil), modestly in Israel (electricity and shale oil), and on the research level also in USA, Australia, Jordan, Morocco, etc.[1]

Thermal analysis (TA) is a convenient analytical technique to study the thermal behaviour and to estimate the thermal characteristics of solid fossil fuels at thermal treatment of them in neutral (pyrolysis) [1–7] or in oxidizing (combustion) [8–16] gaseous atmosphere. The effects of key parameters such as flow rate, nature and purity of gas, particle size and sample amount on the thermal behaviour of oil shale and the reliability of the results obtained were investigated using thermogravimetric apparatus. It was concluded that two analyses carried out under the same experimental conditions should be enough to obtain representative results [8].

During the last two decades, the thermal behaviour of Turkish OS from different deposits has been studied very intensively by Kök et al. [9–11] using thermogravimetric (TG/DTG) and differential thermal (DTA) analysis techniques under non-isothermal heating conditions. In [9], the combustion characteristics of lignite and oil shale samples

T. Kaljuvee (✉) · M. Keelmann · A. Trikkel · R. Kuusik
Laboratory of Inorganic Materials, Tallinn University of
Technology, Ehitajate tee 5, 19086 Tallinn, Estonia
e-mail: tiidu@staff.ttu.ee

---

[1] http://www.worldenergy.org/publications/surveyofenergyresources2007/oilshale.asp

are estimated which showed, depending on the origin of sample, two or three reaction regions: the evaporation of moisture, the release of volatile matter and burning of carbon and, finally, the decomposition of mineral matter. In kinetic calculations, oxidation of lignite and oil shale is described by the first-order kinetics, at that higher activation energy values are obtained at higher reaction temperatures. In pyrolysis experiments [10], one reaction region with two different mechanisms causing mass loss was observed, described as distillation and cracking. In combustion experiments, two distinct exothermic peaks were identified known as low- and high-temperature oxidation. Different methods are used to determine the activation energies of the processes with oil shale samples which vary from 13.1 to 215.4 kJ mol^{-1} in pyrolysis and 13.1 to 408.4 kJ mol^{-1} in combustion experiments [10]. The differences in the activation energies are explained by the different equation parameters and assumptions that these methods are based on. Different degree of maturity and structure of OS also affect the results [11].

Oil shale combustion kinetics was also studied by DSC technique [12, 13]. Experiments were performed in air atmosphere up to 600 °C at five different heating rates. Arrhenius, ASTM and Roger–Morris kinetic methods [12, 13] were used to analyse the DSC data. It was observed that the temperature interval of reactions (low-temperature and high-temperature oxidation region peaks) and burn-out temperatures of the oil shale samples shifted towards higher temperatures as the heating rate increased. The activation energies of the samples vary in the range of 22.4–127.3 kJ mol^{-1} calculated by Arrhenius method [12] and in the range of 131.8–185.3 and 18.5–48.8 kJ mol^{-1} calculated by ASTM and Roger-Morris methods [13], respectively, depending on the oil shale type and heating rate with the trend that the activation energy values in low-temperature oxidation region are higher than those in high-temperature oxidation region.

Thermal behaviour of Huadian OS (China) in combustion and pyrolysis experiments is studied in [14] using thermogravimetric analyzer. It was established that particle size has a little effect on combustion process of oil shale; starting temperature of combustion mass loss and ignition temperature of oil shale decrease with the increase in O_2 concentration in ambient gas; burn-out temperature and maximum rate of combustion mass loss increase with the increase in heating rate. Activation energies calculated using Freeman–Carroll method were for low-temperature stage 27.3–152.2 kJ mol^{-1} and for high-temperature stage 82.8–195.6 kJ mol^{-1} depending on the heating rate.

Combustion characteristics of three semicoke samples formed at retorting of Huadian OS under different retorting temperatures (500, 600 and 700 °C) were studied using thermogravimetric equipment [15]. Kinetic parameters of semicoke combustion were determined by the Coats and Redfern method. Semicoke contains less volatile matter than the corresponding OS. The results proved that volatile matter is released mostly during the low-temperature stage and the fixed carbon during the high-temperature stage, and that the ignition temperature of semicoke samples increased and the burn-out temperature decreased with the increase in the retorting temperature of oil shale. The activation energy values for low-temperature and high-temperature stages were between 118.5 and 233.9 and between 131.7 and 360.1 kJ mol^{-1}, respectively, depending on the final temperature at retorting of oil shale.

In [16], the combustion characteristics of the mixtures of Huadian OS and its semicoke were investigated by means of an on-line TG-FTIR interconnection analyzer. Mainly, three different reaction regions were observed at combustion of most of the samples studied. It was observed that the ignition temperature decreases with an increase in the share of oil shale in the blend resulting in a higher yield of volatile compounds. Kinetic parameters were calculated by binary linear regression method based on Arrhenius kinetic theory. It was observed that activation energies of combustion in the high-temperature region (124.2–421.7 kJ mol^{-1}) were generally higher than those of low-temperature region (48.9–67.2 kJ mol^{-1}), and this could be explained by the differences in the combustion mechanism at different temperatures.

The aim of the present study was to determine thermooxidative decomposition (TOD) characteristics of Estonian oil shale which is very important for evaluation of the possibilities of utilization of Estonian oil shale in future and, besides, to give a comparison of oil shale samples from different deposits.

Table 1 Main characteristics of sample/on dry bases

Content/wt%	EOS	JOS	IOS	MOS	SC
Organic matter + Fixed C	29.7	22.6	17.1	18.5	13.1
Ash	50.5	61.9	60.3	66.4	68.8
$(CO_2)_M$	19.8	15.5	22.6	15.1	18.1
S_{total}	1.63	3.52	2.60	1.97	2.38
S_{pyr}	1.20	0.28	0.88	0.34	0.60
S_{sulph}	0.10	0.12	0.32	0.10	0.44
S_{org}	0.33	3.12	1.40	1.53	0.74
$S_{sulphide}$	Traces	0	0	0	0.60
N	0.53	0.42	0.39	0.50	0.52
H	3.00	2.24	1.46	1.65	1.21
C	28.3	22.2	17.1	16.3	17.9
$(H/C)_{total}^{mole}$	1.27	1.21	1.02	1.21	0.81
Gross calorific value/MJ kg^{-1}	10.24	8.14	4.90	–	4.12

Experimental

Materials

The thermooxidative decomposition of four oil shale samples from Estonia (EOS), Jordan (JOS), Israel (IOS) and Morocco (MOS) and one sample of Estonian oil shale derivative—the solid remainder formed in the production of shale oil at thermal processing of EOS—semicoke (SC) was studied. The samples were prepared according to ASTM standard D2013-03.

Using different methods of analyses, the chemical composition as well as the gross calorific (higher heating) value (calorimeter B-08BM) was determined and is presented for these samples in Table 1. To carry out element

analyses (Vario EL analyzer), the previously air-dried and ground samples were supplementary dried at 105 °C for 24 h.
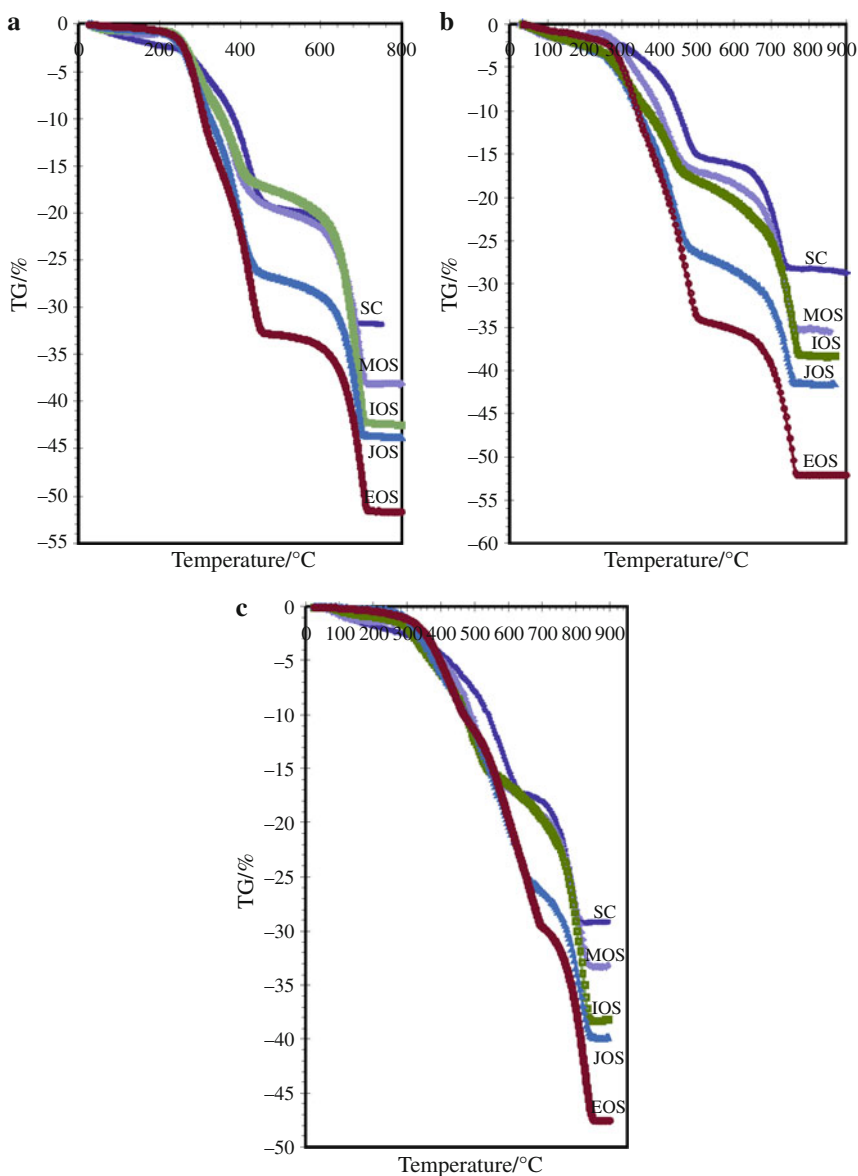
The content of organic matter and fixed carbon (X) in the dry samples was calculated as:

$$X = \left[100 - A^d - (CO_2)_M^d\right], \% \qquad (1)$$

where A^d is the content of ash, %; $(CO_2)_M^d$ is the content of mineral carbon dioxide, %, both on dry bases.

The samples studied are characterized by low content of organic matter—OS between 17 and 30%, and SC 13.1% (Table 1). The content of mineral CO_2 indicated the high content of carbonates (calcite, dolomite) in the samples. The content of sulphur varied from 1.6% (EOS) to 3.5%

Fig. 1 TG curves of samples at a heating rate of 1 °C min^{-1} (**a**), 5 °C min^{-1} (**b**) and 20 °C min^{-1} (**c**)

(JOS) and included pyritic, organic and sulphate sulphur and, additionally, in SC also sulphide sulphur. The content of hydrogen varied in oil shale samples from 1.5% (IOS) to 3.0% (EOS), in SC it was 1.2%.

Significant differences were observed in the values of the mole ratio of $(H/C)^{total}$. For oil shale, it was between 1.02 and 1.27, for SC it was much lower—0.81 (Table 1). The calculated mole ratio of H/C^{org} was also higher for oil shale samples (between 1.49 and 1.62) being for SC 1.12 that indicates higher probability of formation of VOCs at thermal treatment of oil shale as compared to SC samples.
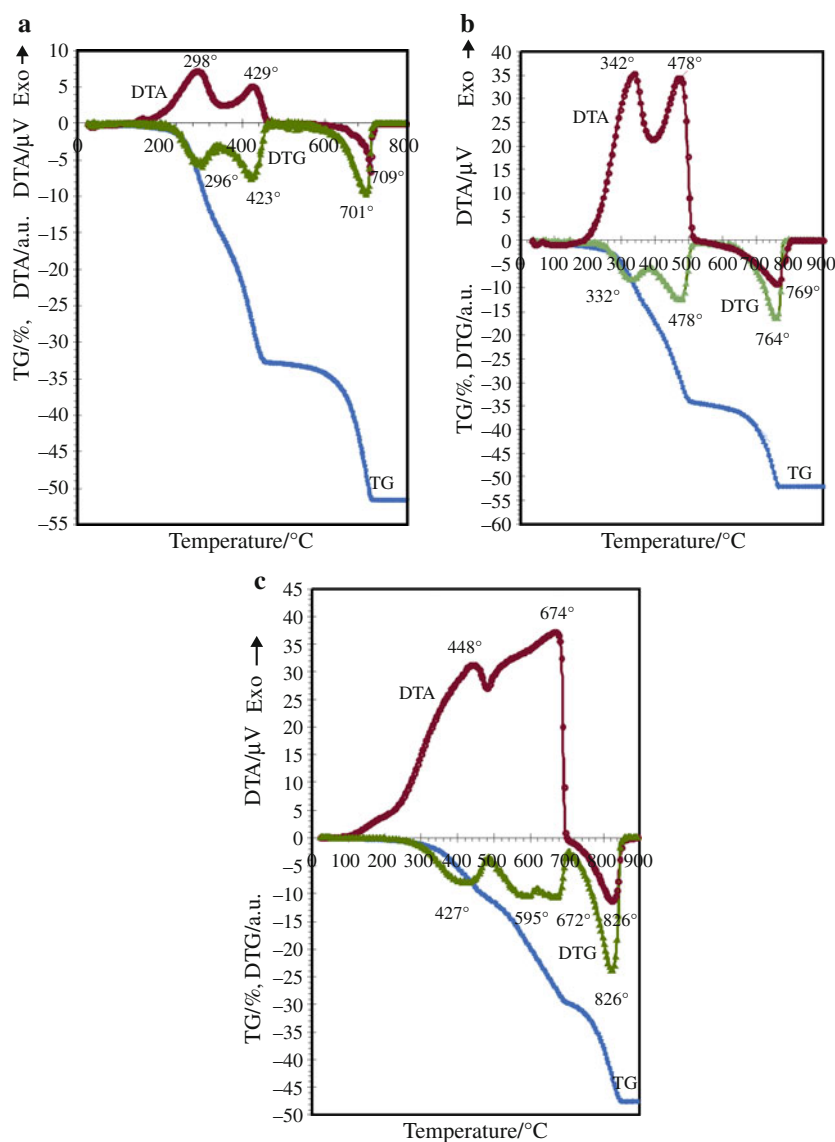
Methods

The experiments with a Setaram Setsys 1750 thermoanalyzer coupled to a Nicolet 380 FTIR Spectrometer by a heated transfer line were carried out under non-isothermal conditions up to 1000 °C at the heating rates of 1, 2, 5, 10 and 20 °C min^{-1} in an oxidizing atmosphere containing 80% of Ar and 20% of O_2. Standard 100-μl alumina crucibles were used, the mass of samples was 15 ± 0.2 mg. To estimate repeatability, all the experiments were performed twice.

FTIR spectra were recorded in the 4000–600 cm^{-1} region with a resolution of 4 cm^{-1} and four scans as an average. The Bio-Rad (Sadtler) KnowItAll search program and Gases&Vapours Database (code GS) and Organics&Polymers Database (code TU, SR) were used.

The differential isoconversional method of Friedman [17] was applied to calculate the kinetic parameters. After baseline correction and normalization the TG signals obtained at different heating rates were processed with the AKTS Advanced Thermokinetics software [18].

Fig. 2 Thermoanalytical curves of EOS at a heating rate of 1 °C min^{-1} (a), 5 °C min^{-1} (b) and 20 °C min^{-1} (c)

Results and discussion

Thermal analyses

Thermooxidative decomposition of OS and SC samples proceeded in three stages. The first stage (step IA, low-temperature oxidation region) is thermooxidation of volatile organic compounds, the second stage (step IB, high-temperature oxidation region) is thermooxidation of heavier part of organic matter (kerogen) and fixed carbon as well as thermooxidation of pyrite and the third stage (step II) is decomposition of carbonates. Additionally, the emission of adsorbed water is observed up to 200–250 °C with the mass loss in the range of 0.9–2.5% (Fig. 1).

The first stage (step IA) of thermooxidation of organic matter for OS and SC lasted, depending on the origin of the sample and the heating rate, up to 330–485 °C (Figs. 1, 2; Table 2) indicating the differences in the content of organic matter of different samples which is the lowest among oil shale samples for MOS and the highest for EOS. The second stage (step IB) of thermooxidation of organic matter lasted up to 465–700 °C. The total mass loss considering both steps of thermooxidation was 16.2–34.3% being definitely the highest for EOS (Table 2).

The third stage (step II) of TOD is mainly related to the decomposition of carbonates and can be followed by the endo-effect with the minimum at 680–826 °C in DTA curves (Fig. 2; Table 2). The mass loss ceased at 705–870 °C (burn-out temperature), the total mass loss at that varied, depending on the origin of the sample and the heating rate, between 31.0 and 52.6%. At higher heating rates, the total mass loss for oil shale samples was reduced by 4–5% and

Table 2 TG-DTA data of experiments

Heating rate/sample	Step IA			Step IB			Step II		
	Interval/°C	DTG/DTA peaks/°C	Mass loss/%	Interval/°C	DTG/DTA peaks/°C	Mass loss/%	Interval/°C	DTG/DTA peaks/°C	Mass loss/%
1 °C min⁻¹									
EOS	200–345	300/290	14.8	345–480	425/425	18.0	480–735	715/690	18.8
JOS	200–340	290/280	11.5	340–475	395/395	14.9	475–720	693/682	17.5
IOS	200–335	290/280	8.9	335–465	388/383	9.2	465–720	693/683	24.3
MOS	200–330	285/275	8.6	330–490	380/384	11.6	490–720	695/690	18.0
SC	200–345	306/290	7.6	345–495	420/417	10.5	495–705	685/680	13.7
2 °C min⁻¹									
EOS	200–365	300/304	14.5	365–485	444/438	17.2	485–745	716/719	20.1
JOS	200–350	305/293	11.8	350–500	413/409	14.2	500–730	698/709	16.4
IOS	200–345	297/297	8.9	245–475	407/399	9.1	475–740	715/717	23.5
MOS	200–340	291/287	7.9	340–495	394/393	11.4	495–730	712/716	19.2
SC	200–360	315/308	7.5	360–510	443/440	9.3	510–735	696/698	13.4
5 °C min⁻¹									
EOS	220–390	332/342	14.6	390–530	478/478	19.7	530–810	745/754	17.7
JOS	220–360	332/327	11.7	360–525	445/442	14.7	525–790	745/754	15.1
IOS	220–370	326/327	9.2	370–505	435/427	9.1	505–785	761/766	20.0
MOS	220–365	329/314	7.9	365–510	424/419	9.6	510–780	747/749	18.0
SC	220–365	326/326	7.4	365–495	474/468	11.0	495–775	727/729	13.1
10 °C min⁻¹									
EOS	220–410	362/368	13.7	410–580	508/513	17.8	580–850	803/803	20.2
JOS	220–380	338/339	10.9	380–585	467/489	15.2	585–835	787/794	14.9
IOS	220–380	326/331	8.8	380–550	453/453	9.1	550–845	800/806	20.5
MOS	220–370	328/319	7.3	370–530	448/439	9.9	530–830	773/773	18.7
SC	220–385	360/342	4.7	385–585	493/502	12.2	585–815	772/779	12.0
20 °C min⁻¹									
EOS	250–485	427/448	11.2	485–700	595/672	18.8	700–870	826/826	17.5
JOS	250–435	366/437	7.9	435–680	565/625	17.9	680–870	813/817	14.1
IOS	250–400	398/411	6.4	400–660	503/516	9.8	660–860	822/825	22.0
MOS	250–430	365/407	5.8	430–605	504/537	10.5	605–865	815/821	17.0
SC	250–485	415/423	6.9	485–650	586/601	10.3	650–830	790/601	12.0

for SC by 3.1% as compared to low heating rates (Figs. 1, 2; Table 2). This effect can be caused by incomplete changes within the mineral part of samples or/and partial binding of the formed and evolved during TOD gaseous species (SO_2, CO_2, HCl) by free Ca, Mg-oxides formed during decomposition of carbonates or by silicates [19–22].

The peaks in DTA and DTG curves of EOS at 298, 429 and 296 °C and 423 °C, respectively (Fig. 2a), heated up at the heating rate of 1 °C min^{-1} and at 342, 478 and 332 °C and 478 °C, respectively (Fig. 2b), heated up at the heating rate of 5 °C min^{-1}, as well as the peaks in DTA curves at 448 and 674 °C, and in DTG curve at 427, 595 and 672 °C at the heating rate of 20 °C min^{-1} (Fig. 2c; Table 2) demonstrate well the complexity of decomposition of organic matter (kerogen) contained in OS. The extremely complicated chemical composition of kerogen in EOS is well proved in [23].

From the differences in the mass losses in low- and high-temperature regions of EOS and SC, it can be concluded that combustion of SC should be more smooth and stable in the case of addition of some EOS. This effect has been well proved by the respective pilot-scale experiments in a fluidized bed furnace [24, 25].

FTIR analysis

The list of gaseous compounds evolved during TOD of different oil shale samples varied slightly depending on the origin of fuel. More differences were observed in the intensities of emissions of these compounds into gaseous phase. The two major gaseous compounds evolved at thermooxidation of fuels were $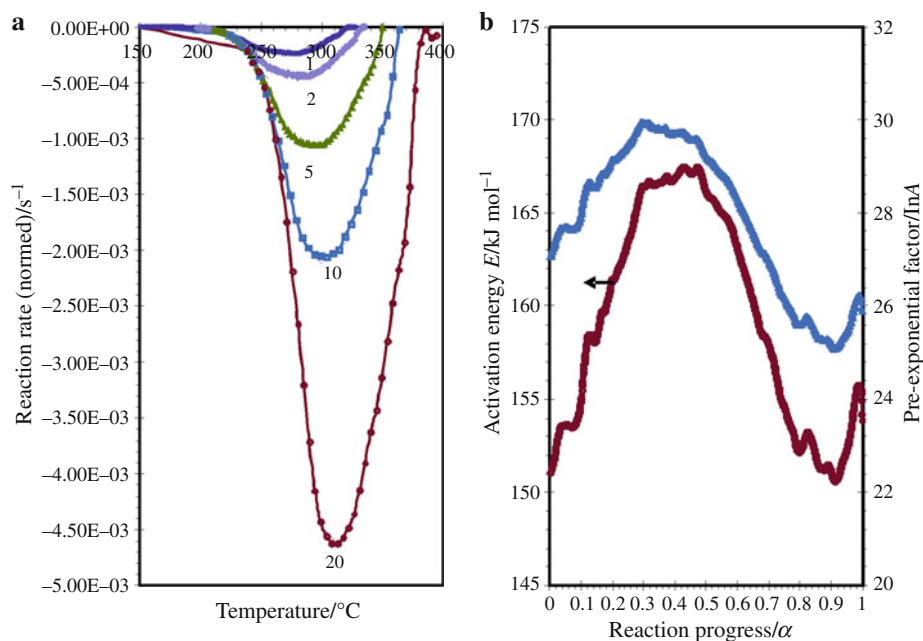CO_2$ and H_2O. In addition, the emission of CO, acetic and formic acids, formaldehyde and acetaldehyde, ketones, SO_2, ethane and chlorobenzene were clearly fixed at thermooxidation of all the samples studied. The emission of ethylene, methanol and ethanol at thermooxidation of IOS and MOS as well as of ethylene, COS, p-xylene and methane at thermooxidation of SC were fixed on the level of traces. No methanol or ethanol was formed at thermooxidation of SC and no NH_3 in the case of MOS [26]. These differences in the emissions during TOD of the samples can be explained by the differences in the content of organic matter, especially, by the differences in its elemental composition which is for IOS, MOS and SC much poorer than for EOS and JOS. Definitely, one of the main factors influencing the complex composition of evolved gases is the content of H (the mole ratio of H/C^{org} in the samples) being the highest for EOS and the lowest for SC (Table 1).

Determination of kinetic parameters

Non-isothermal kinetic study of the TOD processes is complicated in the case of oil shale because of the presence of numerous complex components and their parallel and consecutive reactions. As concluded in the International ICTAC Kinetics project [27], the proper calculation of the kinetic parameters requires series of non-isothermal measurements carried out at different heating rates.

In this study, the differential isoconversional method of Friedman was used which is described by the following equation:

Fig. 3 Reaction rate dα/dt (DTG, normalized signals) as a function of the temperature for different heating rates (a), and activation energy E and pre-exponential factor A determined by Friedman analysis as a function of the reaction progress (b) for the step IA at the thermooxidative decomposition of IOS (the value of the heating rate in °C min^{-1} are marked on the curves)

$$\ln\left(\frac{d\alpha}{dt}\right) = \ln[A(\alpha)f(\alpha)] - \frac{E(\alpha)}{RT}, \tag{2}$$

where α is the degree of conversion, t is time, $f(\alpha)$ is the function dependent on the reaction model, T is the temperature in K, A pre-exponent factor in s^{-1} and R is the gas constant.

The function dependent on the reaction model $f(\alpha)$ becomes a constant at each fixed conversion degree α in Eq. 2, and the relationship between the logarithm of the reaction rate $d\alpha/dt$ and $1/T$ is linear with the slope of E/R.

The calculated reaction rates and kinetic parameters A and E for the TOD of Israeli oil shale are presented in Figs. 3, 4, 5, and for the other samples in Table 3. Herein, step IA presents data for the low-temperature region (depending on the heating rate between 200 and 485 °C) where thermooxidation of volatile organic compounds takes place. Step IB (between 330 and 700 °C) presents data for high-temperature region where thermooxidation of heavier part of organic matter (kerogen), fixed carbon, and pyrite occurs. Step II (between 465 and 870 °C) presents data characterizing decomposition of carbonates.

Fig. 4 Reaction rate $d\alpha/dt$ (DTG, normalized signals) as a function of the temperature for different heating rates (a), and activation energy E and pre-exponential factor A determined by Friedman analysis as a function of the reaction progress (b) for the step IB at the thermooxidative decomposition of IOS
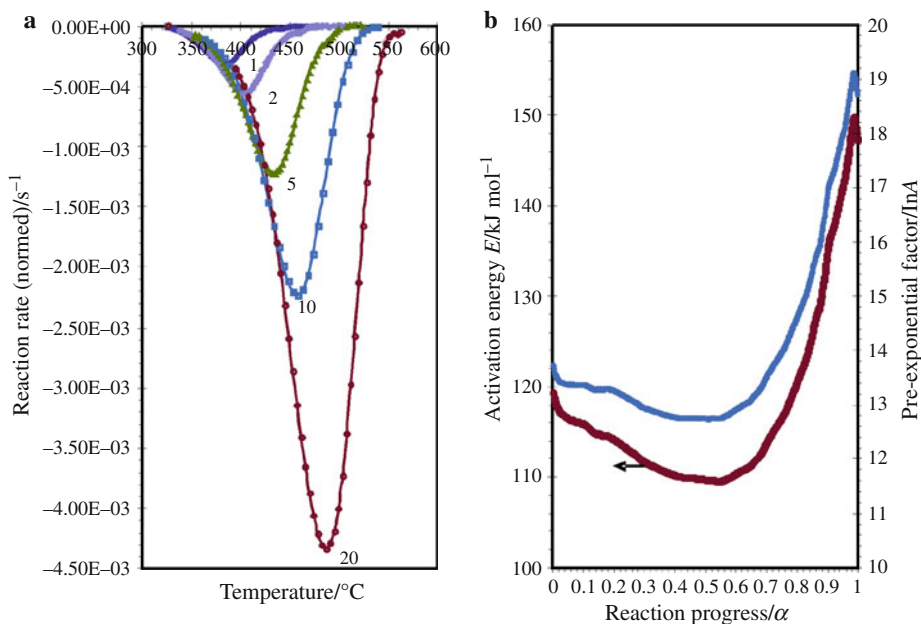

Fig. 5 Reaction rate $d\alpha/dt$ (DTG, normalized signals) as a function of the temperature for different heating rates (a), and activation energy E and pre-exponential factor A determined by Friedman analysis as a function of the reaction progress (b) for the step II at the thermooxidative decomposition of IOS
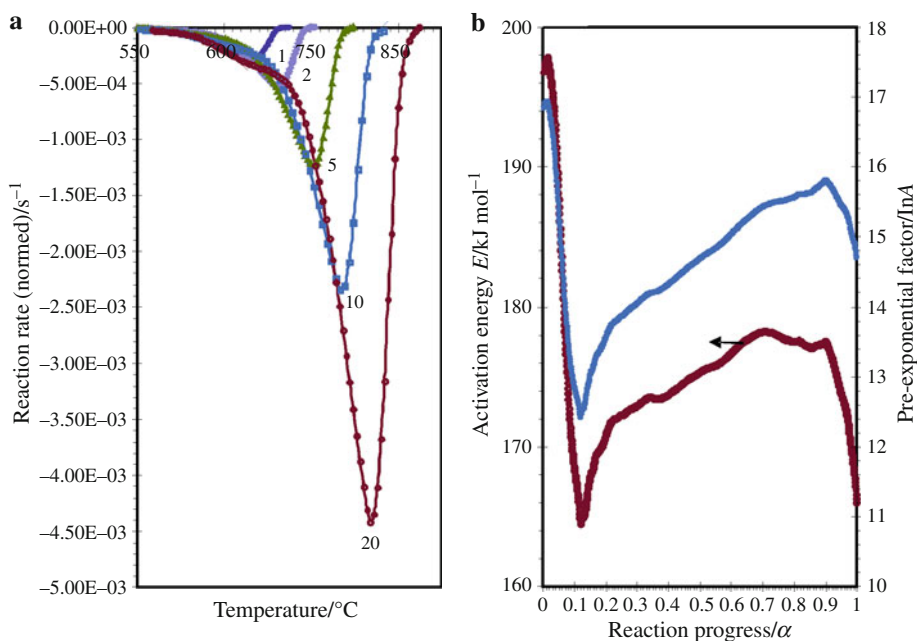
Table 3 The activation energy E/kJ mole^{-1}/and pre-exponent factor $\ln A$ versus reaction progress α

Sample	α																	
	0.1		0.2		0.3		0.4		0.5		0.6		0.7		0.8		0.9	
	E	$\ln A$	E	$\ln A$	E	$\ln A$	E	$\ln A$	E	$\ln A$	E	$\ln A$	E	$\ln A$	E	$\ln A$	E	$\ln A$
Step I																		
EOS, IA	90.3	12.2	80.8	10.2	76.1	9.3	72.9	8.6	70.7	8.2	68.2	7.9	67.0	7.6	53.7	5.6	71.0	8.6
EOS, IB	119.9	12.9	114.3	12.1	110.2	11.6	107.8	11.3	106.5	11.2	105.7	11.2	105.6	11.3	106.7	11.6	108.8	12.1
JOS, IA	141.6	25.0	160.9	29.1	165.8	29.9	138.3	23.5	135.9	22.8	131.1	21.7	137.8	23.0	137.8	23.0	136.2	22.6
JOS, IB	150.3	19.3	142.4	18.0	140.8	17.8	139.4	17.6	141.7	18.0	144.5	18.4	152.4	19.7	165.3	21.7	178.5	23.6
IOS; IA	155.1	28.0	161.4	29.1	166.5	29.9	166.9	29.7	166.1	29.2	163.0	28.3	157.9	27.0	152.3	25.6	151.0	25.1
IOS, IB	115.9	13.4	114.1	13.3	111.7	12.9	110.2	12.8	109.7	12.7	110.4	12.9	113.9	13.5	120.6	14.6	135.4	16.9
MOS, IA	133.9	23.4	130.4	22.5	156.6	28.2	155.7	27.9	136.2	23.4	125.4	20.8	147.1	25.4	127.1	21.1	118.7	19.2
MOS, IB	102.9	11.1	101.3	11.0	100.8	11.1	101.5	11.2	104.1	11.2	104.1	11.6	108.1	12.2	117.8	13.7	129.1	15.3
EOS SC,	98.3	15.5	100.9	16.1	100.6	12.0	99.4	15.6	99.7	15.6	93.0	14.0	77.0	10.4	65.7	7.9	67.3	8.2
EOS SC,	84.0	6.6	82.5	6.6	82.5	6.8	82.0	6.9	81.5	6.9	81.3	6.9	81.6	7.0	82.8	7.3	86.1	7.7
Step II																		
EOS	193.5	16.3	195.9	16.7	188.7	15.9	185.5	15.7	183.5	15.6	183.3	15.7	185.5	16.2	189.5	16.9	187.8	16.9
JOS	181.8	14.7	180.3	14.9	177.5	14.8	176.9	14.9	176.2	15.0	176.9	15.2	178.9	15.7	180.4	16.0	185.0	16.8
IOS	168.3	12.8	170.9	13.6	173.0	14.1	173.8	14.3	175.4	14.7	176.8	15.0	178.2	15.4	177.5	15.6	177.5	15.8
MOS	189.8	16.0	207.0	18.4	212.4	19.1	207.2	18.6	202.2	18.1	199.1	17.9	197.2	17.9	196.3	17.9	191.5	17.5
EOS SC	182.7	15.5	185.8	16.1	185.6	16.2	184.8	16.3	184.3	16.4	184.1	16.5	184.2	16.7	184.4	16.9	184.4	17.1

For step IA, the value of activation energy in the range of conversion level $0.1 < \alpha < 0.9$ varied for EOS and SC from 53.7 to 100.9 kJ mole^{-1} (pre-exponential factor A between 2.7×10^2 and 9.8×10^6 s^{-1}) and for the other oil shale samples from 118.7 to 166.9 kJ mole^{-1} (pre-exponential factor A between 2.2×10^8 and 9.7×10^{12} s^{-1}). For step IB in the same range of α, the value of activation energy varied for oil shale samples from 100.8 to 178.5 kJ mole^{-1} (pre-exponential factor A between 6.0×10^4 and 1.8×10^{10} s^{-1}), and for SC from 81.3 to 86.1 kJ mole^{-1} (pre-exponential factor A between 7.4×10^2 and 2.2×10^3 s^{-1}). At that, for EOS (over the full range of α) and for JOS (α range 0.4–0.9), which are characterized by higher content of volatile organic compounds as compared to the other samples, the value of activation energy in the low-temperature oxidation region was lower than in the high-temperature oxidation region. This was contrary to the other samples studied. For step II, the value of activation energy varied between 168.3 and 212.4 kJ mole^{-1} (pre-exponential factor A between 3.6×10^5 and 2.0×10^8 s^{-1}), but for a definite sample, its variations with conversion level were notably less in this step as compared to step IA or IB.

compounds (depending on the heating rate between 200 and 485 °C), secondly, thermooxidation of heavier part of kerogen and fixed carbon (up to 465–700 °C) and finally decomposition of carbonates (up to 705–870 °C). In addition, the emission of adsorbed water takes place at temperatures up to 250 °C.

The number of compounds evolved is bigger and, particularly, their concentration in the gaseous phase is much higher in the case of EOS and JOS as compared to IOS, MOS and SC. The value of activation energy E in the low-temperature oxidation region (step IA) was for EOS and JOS lower than that in the high-temperature oxidation region (step IB), which was contrary to IOS, MOS and SC.

The results obtained indicate that the thermooxidative decomposition of oil shale and semicoke has a multi-step mechanism, being the most complicated for EOS and JOS which are characterized by higher content of organic matter as compared to the other samples studied and they can be used for selecting composition of fuel mixtures in the combustion of low quality solid fossil fuels including coal and semicoke.

Conclusions

The thermooxidative decomposition of oil shale proceeds in three stages: first, thermooxidation of volatile organic

References

1. Johannes I, Zaidentsal A. Kinetics of low-temperature retorting of kukersite oil shale. Oil Shale. 2008;25:412–25.

2. Olivella MA, de las Heras FXC. Nonisothermal thermogravimetry of Spanish fossil fuels. Oil Shale. 2006;23:340–55.
3. Berkovich AJ, Young BR, Levy JH, Schmidt SJ, Ray A. Thermal characterization of Australian oil shales. J Therm Anal Calorim. 1997;49:737–43.
4. Torrente MC, Galán MA. Kinetics of the thermal decomposition of oil shale from Puertollano (Spain). Fuel. 2001;80:327–34.
5. Aboulkas A, El Harfi K. Study of the kinetics and mechanisms of thermal decomposition of Morrocan Tarfaya oil shale and its kerogen. Oil Shale. 2008;25:426–43.
6. Qing W, Hongpeng L, Baizhong S, Shaohua L. Study on pyrolysis characteristics of Huadian oil shale with isoconversional method. Oil Shale. 2009;26:148–62.
7. Kök MV, Pamir R. Pyrolysis kinetics of oil shales determined by DSC and TG/DTG. Oil Shale. 2003;20:57–68.
8. Lisboa ACL, Watkinson AP. Operating conditions for oil shale thermogravimetry. Powder Technol. 1999;101:151–6.
9. Kök MV, Pokol G, Keskin C, Madarász J, Bagci S. Combustion characteristics of lignite and oil shale samples by thermal analysis techniques. J Therm Anal Calorim. 2004;76:247–54.
10. Kök MV, Iscan AG. Oil shale kinetics by differential methods. J Therm Anal Calorim. 2007;88:657–61.
11. Kök MV, Pamir MR. Comparative pyrolysis and combustion kinetics of oil shales. J Anal Appl Pyrol. 2000;55:185–94.
12. Kök MV. Heating rate effect on the DSC kinetics of oil shale. J Therm Anal Calorim. 2007;90:817–21.
13. Kök MV, Pamir MR. ASTM kinetics of oil shales. J Therm Anal Calorim. 1998;53:567–75.
14. Han XX, Jiang XM, Cui ZG. Thermal analysis studies on combustion mechanism of oil shale. J Therm Anal Calorim. 2006;84: 631–6.
15. Qing W, Baizhong S, Xiahua W, Jingru B, Jian S. Influence of retorting temperature on combustion characteristics and kinetic parameters of oil shale semicoke. Oil Shale. 2006;23:328–39.
16. Qing W, Baizhong S, Xiahua W, Jingru B, Jian S. Study on combustion characteristics of Huadian oil shale and semicoke. Oil Shale. 2007;24:135–45.
17. Friedman HL. Kinetics of thermal degradation of char-forming plastics from thermogravimetry. Application to phenolic plastic. J Polym Sci. 1965;6C:183–95.
18. AKTS Softwear Setaram Instruments. A global solution for kinetic analysis and determination of the thermal stability of materials. Switzerland: AKTS AG; 2006. p. 88.
19. Kaljuvee T, Kuusik R. Emission of sulphur dioxide during thermal treatment of fossil fuels. J Therm Anal Calorim. 1999;56: 1243–51.
20. Kaljuvee T, Kuusik R, Radin M, Bender V. Carbon dioxide binding in the heterogeneous systems formed at combustion of oil shale. 4. Reactivity of ashes towards acid gases in the system fly ash-flue gases. Oil Shale. 2004;21:13–26.
21. Xie W, Liu K, Pan WP, Riley JT. Interaction between emissions of SO_2 and HCl in fluidized bed combustors. Fuel. 1999;78: 1425–36.
22. Partanen J, Backman P, Backman R, Hupa M. Adsorption of HCl by limestone in hot flue gases. Part III: simultaneous adsorption with SO_2. Fuel. 2005;84:1685–94.
23. Lille Ü. Current views on the origin of Estonian kukersite kerogen. Oil Shale. 2002;19:3–18.
24. Kuusik R, Martins A, Pihu T, Pesur A, Kaljuvee T, Prikk A, Trikkel A, Arro H. Fluidized bed combustion of oil shale retorting solid waste. Oil Shale. 2004;21:237–48.
25. Trikkel A, Kuusik R, Martins A, Pihu T, Stencel JM. Utilization of Estonian oil shale semicoke. Fuel Proc Technol. 2008;89: 756–63.
26. Kaljuvee T, Pelt J, Radin M. TG-FTIR study of gaseous compounds evolved at thermooxidation of oil shale. J Therm Anal Calorim. 2004;78:399–414.
27. Brown ME, Maciejewski M, Vyazovkin S, et al. Computational aspects of kinetic analysis. Part A: the ICTAC kinetics project-data, methods and results. Thermochim Acta. 2000;355:125–43.